Investigation of a Photovoltaic Thermal-Direct Expansion Solar-Assisted Heat Pump (PVT-DXSAHP) Collector with Different Photovoltaic Characteristics in Cold Climates

*Adam Anastas & Aggrey Mwesigye**

Department of Mechanical and Manufacturing Engineering, University of Calgary, Calgary, AB

https://doi.org/10.33697/ajur.2025.133

Student: adam.anastas@ucalgary.ca
*Mentor: aggrey.mwesigye@ucalgary.ca**

ABSTRACT
In this paper, the performance of a direct expansion solar-assisted heat pump (DX-SAHP) with a photovoltaic thermal (PVT) collector made with different solar cells was investigated. A thermodynamic model of a direct expansion solar-assisted heat pump with a PVT collector and a 180 L water tank for thermal energy storage was developed. The model was implemented in MATLAB, with the CoolProp library for the retrieval of working fluid thermodynamic properties. The solar collector cells considered were ®Solartech, ®LG, ®Prime, ®VOLT, and ®VSUN. The performance of the system is characterized by the coefficient of performance, thermal efficiency, electrical efficiency, heat pump ratio and auxiliary heat ratio. The highest average coefficient of performance of the heat pump was with ®Solartech solar cells on a sunny day in winter was 4.08 , and 7.91 on a sunny summer day. On a cloudy summer day, the ®Prime solar cell had the highest average coefficient of performance at 6.45. The highest electrical efficiency of the collector was observed with ®Prime solar cells, with an efficiency of 14.4%, 16.5% and 13.6%, respectively, from a sunny day in winter, a sunny day in summer and a cloudy day in the summer. The highest thermal efficiency was obtained by ®Solartech solar cells for all weather conditions. With a collector area of 5 m^2 and a consumer load of 0.001 kg/s, the heat pump meets an average of 15.6% of the total heat needed for domestic hot water demand on a sunny winter day. This increases to 38.2% and 49.0% on cloudy and sunny summer days, respectively.

KEYWORDS
Coefficient of Performance; Direct Expansion; Heat Pump Ratio; Photovoltaic Thermal ; Water Heating; Solar-Assisted Heat Pump

INTRODUCTION

In 2019, Canada's residential water heating use accounted for 263.9 PJ of energy or about 17% of the total energy in the residential sector. About 12.4 million Canadians have standard water heaters and 5.5 million of those water heaters use natural gas as the energy source, while 5.6 million use electricity.[1] This leads to about 11.13 megatons of carbon dioxide equivalent emitted from residential water heating.[2] To meet this energy demand with minimal emissions, alternative and clean energy technologies are essential.

Heat pumps are emerging as a clean alternative to conventional systems. When powered by clean electricity, they have the potential to meet the heating and cooling needs with minimum emissions. However, in cold climates, the performance of heat pumps degrades with decreasing outdoor air temperatures. Thus, combining or replacing heat pumps with solar thermal collectors is emerging as an effective means of enhancing their performance. The direct expansion solar-assisted heat pump (DX-SAHP) is a class of solar-assisted heat pump (SAHP) systems that uses a solar collector directly as the evaporator of the heat pump system. The heated refrigerant vapor is then compressed to a higher pressure and temperature and used to heat a water tank for specific residential applications. A prototype DX-SAHP developed in the Sustainable Thermal Energy Systems Research lab at the University of Calgary by Elgamal et al. this prototype consists of a 2.3 m^2 flat solar plate with no glazing, a scroll compressor rated at 3500 rpm, an electronic expansion valve, copper piping at a length of 25 m, a pitch of 19.05 mm and bend diameter of 100 mm and hot water storage tank. The theoretical results of this setup were obtained using the combined Hottel-Whillier-Bliss equations, and the first law of thermodynamics showed coefficients of performance (COP) from 3.4 - 4.5.[3] The results of experimental tests conducted on the prototype achieved a COP of 3.1 on a sunny winter day and raised the water tank temperature from 16.1 ^oC to 50.3 ^oC in 4.5 hours. While on an overcast summer day, the COP average was 3.0, and the water tank temperature increased from 27.3 ^oC to 49.5 ^oC in 3.5 hours.[4] Bonding the tubing to the collector is one of the important factors that affect the performance of

evaporator in DX-SAHPs. Moreover, the tubing pattern used can influence performance of the heat pump. Different flow patterns have been used for plate-and-tube and roll bond collectors. Using a fractal T-shape pattern, the coefficient of performance (COP) and heating capacity of the heat pump enhanced the system by 14.6% and 17.3% respectively compared to the parallel channel pattern. A similar but smaller improvement was achieved with a honeycomb-shaped pattern in the same study, with an increase in the COP of 5.9% and an increase in the heat capacity of 6.2%.[5] A different study looked at SAHP where the collector was adapted to include a heat pipe in the collector itself and to work in two modes. One of these modes is called the heat pipe mode, which moves the refrigerant straight to the condenser during times of large solar insolation; the other mode is a heat pump which didn't bypass the compressor before going into the condenser.[6]

Solar collectors are based on the flat plate collector technology which are easy to design and relative less expensive to make, however they don't take advantage of the simultaneous generation of both electric and thermal energy thus leading to lower useful energy efficiencies. There are four main types of solar collectors currently used in solar-assisted heat pumps: flat solar collectors, evacuated tube solar collectors, parabolic solar trough collectors and photovoltaic-thermal (PV-T) collectors. The flat plate solar collector is the simplest collector, mostly rectangular in shape, with a collector tube on the back of the plate with insulation under it. The evacuated tube solar collector is like the plate solar collector. However, the space in between the absorber plate and the glass cover is a vacuum to minimize heat loss, which is applicable in cold climates. Parabolic solar trough collectors are shaped like a parabola, which helps concentrate the solar light/radiation to a line, increasing the intensity of the light to a line where the absorber tube will sit and collect the heat. PV-T collectors add photovoltaic (PV) cells to the absorber surface where all the solar light concentrates while having collector's tubes behind the collector with the refrigerant to extract what is not collected by the PV cells to be then used in a heat pump, water or air heating system. Thus, PV-T solar collectors provide additional benefits of generating electricity that can be used to meet part of the energy required by the heat pump, water or air heating system.
An interesting study used a façade integrated PVT water heating system to explore the use of building-integrated solar technology for water heating. They showed that the electrical efficiency reached an average of 8.56% and a thermal efficiency of 38.9% late in the summer for Hong Kong.[7] The same group studied a PV-thermal air system built into the house and examined its winter performance. The polycrystalline silicon cell modules had an electrical conversion of about 11.2% to 11.4%, depending on whether there was a Teflon cover on the cells. Amorphous silicon cells had a reduction in the electrical efficiency of about 3.6% compared to polycrystalline silicon cells. The thermal efficiency was about 29.2% without glass covers and 36.9% with glass covers.[8]

Modifications of PV/T collectors enhance the performance of combined PV/T water collector thermodynamic efficiencies. PV/T collectors that added reflectors showed that the ideal angle of the collector surface should be 45° horizontal from the ground and the reflectors should be placed at different angles in the season: 5° in December and 38° in June perpendicular to the collector surface to optimize the thermodynamic efficiency of a PV/T water collector.[9] Kalogirou et al. looked at PV/T systems in Nicosia, Athens and Madison using two types of photovoltaic cells in their simulations.[10] They used polycrystalline and amorphous silicon cells connected to a water heat extraction unit and tested them against PV modules of similar cells. Results showed that the overall performance of the photovoltaic modules increased and that these hybrid units had a better chance of success compared to any of the PV amorphous or polycrystalline modules. They showed the systems to be more economically viable for locations across Nicosia and Athens. The study showed that the type of PV cells significantly affects the performance and cost of the system.

Besides the type of cells, the absorber tube configuration on the PV-T collector is an important factor in determining the overall system performance. Kazem et al. performed a study in Oman, looking at the electrical, thermal and overall efficiencies of different flow configurations of a PV-T water cooling system.[11] Their results showed that the spiral flow type gave an improved thermal performance while also achieving 9.1% electrical efficiency. The overall efficiencies were about 35% for the spiral flow type, the highest of all the PVT systems studied by Kazem's research group. A similar study numerically and experimentally investigated the type of channel configurations (serial, parallel, bionic) for roll–bond heat exchangers.[12] They found that the outlet water temperature of the bionic configuration was the lowest and had the lowest pressure drop. All PV-T water collector systems had improved electrical efficiency compared to a PV-only module.

One of the first studies looking at integrating PVT collectors and heat pumps was called an integrated-type solar-assisted heat pump. They found that the system was 76% more thermally efficient than solar water collectors.[13] Given the benefits of PV-T water collector heating and cooling systems, using them in direct expansion heat pump systems results in better performance and promising economics. As such, several researchers are looking into direct-expansion solar-assisted heat pumps with photovoltaic cells. Ammar et al. showed that using a photovoltaic/thermal–direct-expansion solar-assisted heat pump with R134a as the refrigerant, the electrical efficiency reached about 11.9% percent with a maximum hourly thermal efficiency of 88.7% and an average COP of 6.14.[14] Another study found that a PVT-heat pump provided a maximum COP of 8.4, with a maximum condenser capacity of 2.4 kW. The average electrical efficiency was 13.7% with the cooling effect of the refrigerant.[15] A similar

study with a double glass cover on the collector showed a higher electrical efficiency of 15.2% and a COP of 2.96.[16] James et al. used a variable frequency drive (VFD) compressor-based PV-THPWH system in Calicut City, India.[17] They found that the VFD compressor control feedback system improved the energy performance and life by making the mass flow rate of the refrigerant proportional to the evaporator load.

As the literature shows, several researchers have investigated DX-SAHP, different configurations of PVT collectors, and their combinations with heat pumps and solar water collectors. However, the study of commercially available photovoltaic cells on the collectors of DX-SAHPs in cold climates has not been studied in detail. Especially for climates that are cold and have yet to open up to its significant solar resources, such as the city of Calgary in Alberta. The aim of this study was to develop a model of a PVT-DXSAHP and investigate its performance in a cold climate with different photovoltaic cells on its collector.

METHODS AND PROCEDURES

Description of the system

Figure 1 represents the configuration of the PVT-DXSAHP system, which comprises a heat pump with a PVT collector, compressor, condenser and expansion valve. Connected to the condenser is a water loop that uses a pump to drive the heated water inside the water tank. Using the heat from the condenser, water in the tank is heated up and used for residential applications at a temperature of 50 ^{o}C when needed.

The refrigerant starts as a two-phase liquid when it exits the expansion valve (4); as it passes through the PVT collector or the evaporator, where it gains heat from solar radiation or surroundings, causing the refrigerant to change state to a superheated vapor state (1). When it passes through the compressor, the refrigerant temperature and pressure increase to a superheated vapor (2). The refrigerant then goes into a condenser where it transfers heat to the water loop, losses energy and changes its phase to a sub-cooled liquid (3). This cycle continues, provided the heat pump is in operation.

Figure 2 provides the temperature-entropy (T-s) diagram detailing the heat pump processes. Process 1-2s represents the ideal isentropic compression process, while 1-2 shows the actual compression process. Process 3-4 represents an enthalpic process across the thermostatic expansion valve.

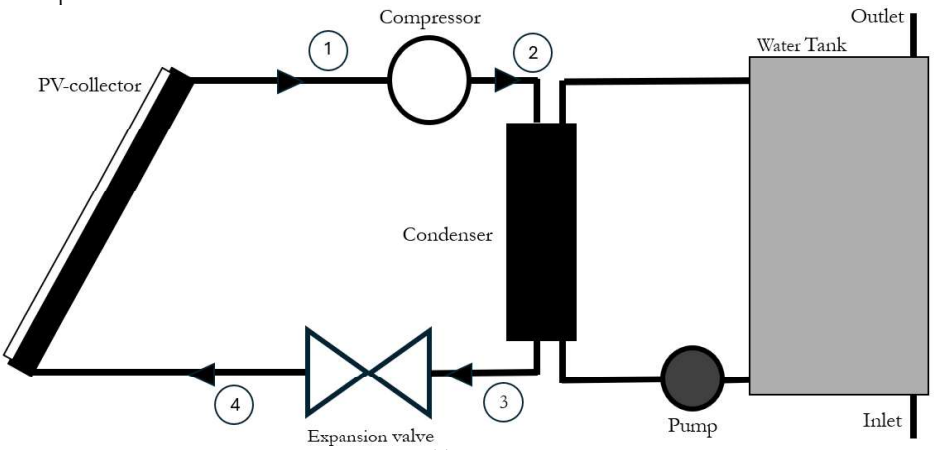

Figure 1. PVT-DXSAHP system

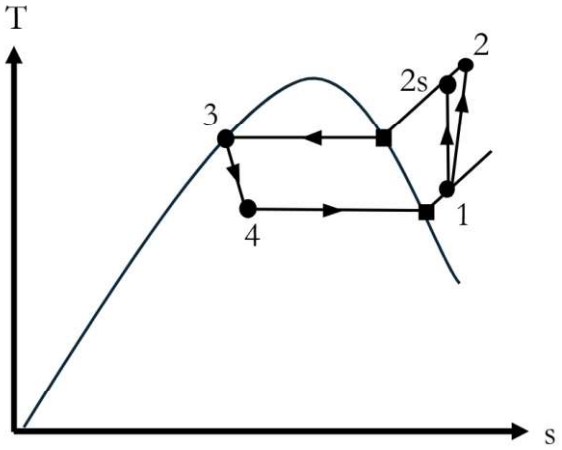

Figure 2. Thermodynamic process of the heat pump system

Solar Cell Types

Table 1 shows the photovoltaic solar cells used in this study. The solar cells produced by ®LG, ®Prime, ®VOLT, and ®VSUN are all monocrystalline silicon solar cells but with different efficiencies. ®Solartech solar cells are polycrystalline silicon solar cells. The reference efficiency indicates the efficiency of the solar cell at 1 AM at 25 °C. The temperature coefficient helps indicate the trend of the solar cell's efficiency as it varies with temperature.

Solar Cell	Temperature Coefficient, β_r (1/K)	Reference Efficiency	References
®LG	-0.0033	20.9%	18
®Solartech	-0.0046	13.5%	19
®Prime	-0.0030	25.0%	20
®VOLT	-0.0039	22.9%	21
®VSUN	-0.0032	20.2%	22

Table 1. Table of simulated solar cells with their characteristics of temperature coefficient and reference efficiency.

Meteorological Data and Load Profile

Figures 3, **4** and **5** show meteorological data for Calgary, Alberta used in this study. A sunny winter day, a sunny summer day and a cloudy sunny day in summer day, were respectively used in this study. In the MATLAB simulation, a constant water load of 0.001 kg/s from 8 am to 8 pm was assumed to evaluate the performance of this PVT-DXSAHP system. A constant water load was used because it provides a general approximation of the residential water use during a 12-hour period. This data was used as an input parameter in the analysis of the PV-DXSAHP system.

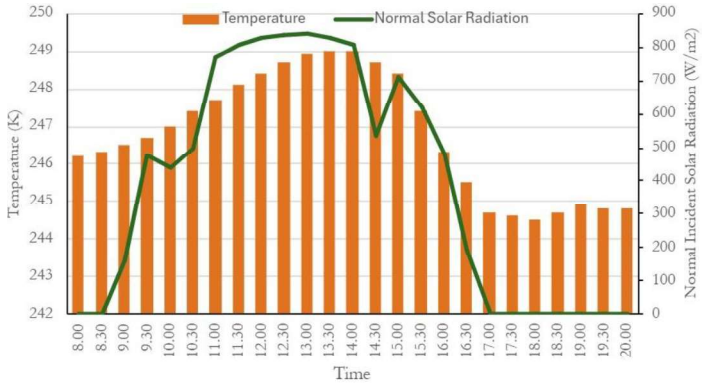

Figure 3. Temperature and solar radiation on a tilted surface in Calgary, Alberta, 2022, January 4th.

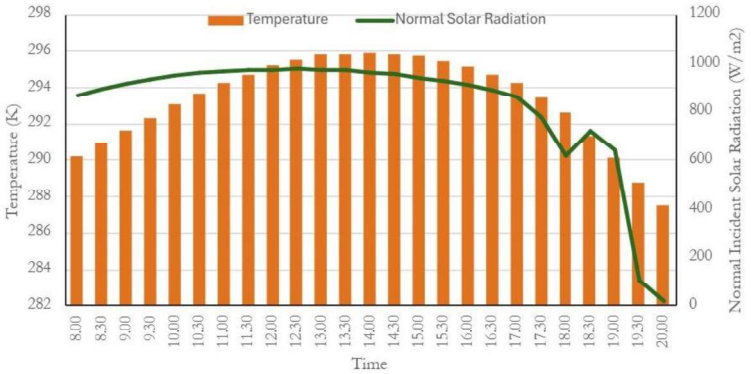

Figure 4. Temperature and solar radiation on the tilted surface in Calgary, Alberta, 2022, June 10th.

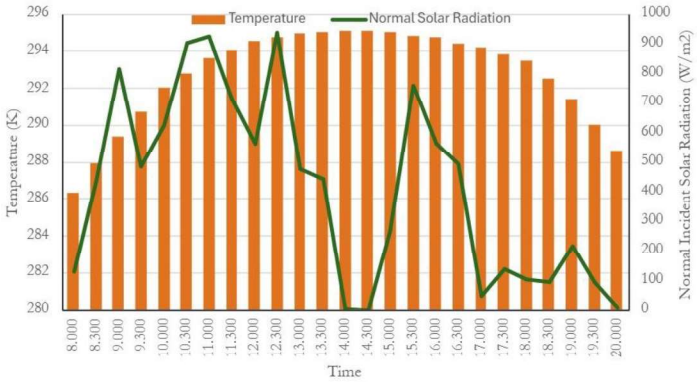

Figure 5. Temperature and solar radiation on the tilted surface in Calgary, Alberta, 2022, June 18th.

Mathematical Model

In this section, the mathematical model developed in MATLAB that describes the photovoltaic/thermal–direct-expansion solar-assisted heat pump is shown. In the later sections, the validation procedure used for this model is reported. This model follows similar assumptions in Bardia Thesis.[23] The mathematical model is also extended based on the Hotel-Whillier model for photovoltaic/thermal flat-plate collectors.[24] All components are assumed to operate steadily, except the water tank, where temperature changes with time.

The additional assumptions are:

i. Pressure drop in the refrigerant lines is negligible.
ii. Isenthalpic throttling process through the expansion valve.
iii. The heat losses through the edge of the collector are negligible.
iv. The properties of the collector are independent of temperature.
v. Heat losses from the heat exchanger/condenser to the ambient are negligible.
vi. The power input into the water pump is negligible compared to the compressor power input.
vii. In the evaporator, the tube temperature is equal to the evaporating temperature.

First, the energy picked up by the refrigerant through the evaporator is,

$$\bar{Q}_u = \bar{m}_r(h_1 - h_4) \qquad \textbf{Equation 1.}$$

Where $\bar{m}_r$ is the mass flow rate of the refrigerant. h_1 is the enthalpy of the refrigerant leaving the collector while h_4 is the enthalpy of the refrigerant entering the collector. This process from 1 to 4 is shown in **Figure 2**.
The volumetric efficiency of the compressor is given by.[25]

$$\eta_{vol} = 0.959 - 0.006422\frac{P_c}{P_e} \qquad \textbf{Equation 2.}$$

Where P_c is the pressure of the refrigerant through the condenser and P_e is the pressure of the refrigerant through the evaporator. The mass flow rate of the refrigerant can be calculated from the knowledge of compressor characteristics as

$$\bar{m}_r = \frac{\eta_{vol} n V_d \rho_r}{60}$$ **Equation 3.**

n is the speed of the compressor, V_d is the volumetric displacement of the compressor and ρ_r is the density of the refrigerant.

The work input into the compressor is given by equation (4), process 1-2, shown in the T-s diagram in **Figure 2**.

$$W_c = \frac{\dot{m}_r(h_2 - h_1)}{\eta_{is}}$$ **Equation 4.**

Where η_{is} is the isentropic efficiency of the compressor.[25]

$$\eta_{is} = 0.874 - 0.0135\frac{P_c}{P_e}$$ **Equation 5.**

Where P_c is the condenser pressure and P_{evap} is the evaporator pressure.

The thermal loss that occurs at the top of the photovoltaic cells without glazing is the sum of the radiation and convective losses.

The respective heat transfer coefficients are given by **Equations (6)** and **(7). Equation(6)** is found in [26] and **Equation (7)** is found in Bardia's Thesis.[23]

$$h_{r,PV-amb} = \varepsilon_{PV}\sigma({T_{PV}}^2 + {T^2}_{amb})(T_{PV} + T_{amb})$$ **Equation 6.**

$$h_{c,PV-amb} = 2.8 + 3u_{amb}$$ **Equation 7.**

Where **Equation (6)** is the radiative heat transfer coefficient representing the loss that occurs from the photovoltaic cells on the top of the collector to the ambient air, **Equation (7)** is the convective heat loss coefficient from the photovoltaic cells to the ambient air.

The thermal resistance arising from convection and radiation that occurs in the ambient air

$$R_{r-c} = \frac{1}{h_{r,PV-amb} + h_{c,PV-amb}}$$ **Equation 8.**

The conduction thermal resistance which occurs through the photovoltaic cell is

$$R_{PV} = \frac{\delta_{PV}}{k_{PV}}$$ **Equation 9.**

Where k_{PV} is the thermal conductivity of the photovoltaic cell and δ_{PV} is the thickness of the of the photovoltaic cell on the collector.

The bottom heat loss coefficient is

$$U_{Bottom} = \frac{k_b}{\delta_b}$$ **Equation 10.**

Where k_b is the thermal conductivity of the insulation or padding on the back of the collector, δ_b is the thick of that padding or insulation.

The total heat loss coefficient for the collector is

$$U_L = \frac{1}{R_{c-r} + R_{PV}} + U_{Bottom}$$ **Equation 11.**

Combining **Equation (6)** through **(7)** into **Equation (8)** and **Equations (9)** and (**10)** all into **Equation (11)**

$$U_L = \frac{1}{\frac{1}{h_{r,PV-amb} + h_{c,PV-amb}} + \frac{\delta_{PV}}{k_{PV}}} + \frac{k_b}{\delta_b}$$ **Equation 12.**

The electrical collector efficiency can be calculated as,

$$\eta_c = \eta_r[1 - \beta_r(T_{PV} - T_r)]$$ **Equation 13.**

Where η_r is the reference efficiency of the collector tested at 1.5 AM at 25°C. β_r is the temperature coefficient of the photovoltaic cells, and T_r is the reference temperature.

The current/local ambient collector electrical efficiency can be calculated by

$$\eta_{amb} = \eta_r[1 - \beta_r(T_{amb} - T_r)] \quad \textbf{Equation 14.}$$

This is a condition where the PV cells are at the temperature of the ambient air. Both **Equation (13)** and **(14)** come from Kalogirou et al.[27]

For photovoltaic thermal collectors, the modified heat loss coefficient can be calculated by Florschuetz.[24]

$$\bar{U}_L = U_L - \frac{S}{\alpha}\eta_c\beta_r \quad \textbf{Equation 15.}$$

Where α is the absorptivity of the whole array of photovoltaic cells on the collector.

The modified solar radiation can be calculated according to Florschuetz as,[24]

$$\bar{S} = S(1 - \frac{\eta_{amb}}{\alpha}) \quad \textbf{Equation 16.}$$

h_{fi} is the coefficient of heat transfer of the two-phase refrigerant given by Turaga et al.[28]

$$h_{fi} = \frac{0.0082k_l}{D_i}\left(\frac{J\,\Delta x h_{fg}}{L}\right)^{0.4} \quad \textbf{Equation 17.}$$

Where k_l is the thermal conductivity of the refrigerant; Re is the Reynolds number, J is the design constant, Δx is the quality difference between the phase of the outlet and the exit of the collector and h_{fg} is the latent heat of the refrigerant.

The collector efficiency factor is given by Duffie and Beckmann.[26]

$$F' = \frac{1/\bar{U}_L}{W[\frac{1}{\bar{U}_L[D+(W-D)F]} + \frac{1}{C_b} + \frac{1}{\pi D_i h_{fi}}]} \quad \textbf{Equation 18.}$$

W is the distance between each tube, D is the diameter of the absorber tube, C_b is the conduction bond conductance between the absorber tube and the collector plate. F is the fin efficiency of the collector defined by Duffie and Beckman as,[26]

$$F = \frac{tanhtanh\,[\,m(W-D)/2]}{m(W-D)/2} \quad \textbf{Equation 19.}$$

Where m is given by

$$m = \sqrt{\frac{\bar{U}_L}{k_P\delta_P}} \quad \textbf{Equation 20.}$$

In which, k_P is the thermal conductivity of the collector plate, and δ_P is the thickness of the collector plate.

The modified useful heat of the collector is then calculated as

$$\bar{Q}_u = A_c[\bar{S}(1 - \eta_c) - \bar{U}_L(T_P - T_a)] \quad \textbf{Equation 21.}$$

Instead of the plate temperature, the evaporator temperature can be used with a modified equation as

$$\bar{Q}_u = F'A_c[\bar{S}(1 - \eta_c) - \bar{U}_L(T_e - T_a)] \quad \textbf{Equation 22.}$$

An energy balance between the plate and the refrigerant in the absorber tube gives

$$\bar{Q}_u = \frac{L(T_p - T_e)}{\frac{1}{\pi D_i h_{fi}} + \frac{1}{C_b}} \quad \textbf{Equation 23.}$$

The electrical energy which is extracted from the collector plate can be calculated by

$$Q_e = \bar{S}A_c - Q_u - \bar{U}_L A_c(T_p - T_a) \quad \textbf{Equation 24.}$$

The energy loss which occurs throughout the ambient air and the aluminum plate of the collector can be identified as

$$\frac{T_P - T_a}{R_{r-c} + R_{PV}} = \frac{T_{PV} - T_p}{R_{PV}} \quad \textbf{Equation 25.}$$

Using algebra in **Equation (25)**, the cell temperature can be obtained and calculated. Examining the steady state flow of the thermal energy transferred into the refrigerant without ambient losses, we can write the following equations. The energy transferred to the water in the tank is

$$Q_c = \dot{m}_w C_p (T_{wo} - T_w) \quad \textbf{Equation 26.}$$

Where T_{wo} and T_w are the outlet water temperature of the water heat exchanger and the water tank inlet temperature.

The heat loss from the condenser, however, can be expressed as

$$Q_c = U_c A_C \Delta T_{lm} \quad \textbf{Equation 27.}$$

The term ΔT_{lm} is the mean log temperature of the heat exchanger in the condenser.

$$\Delta T_{lm} = \frac{(T_2 - T_{wo}) - (T_c - T_w)}{lnln\left(\frac{T_2 - T_{wo}}{T_c - T_w}\right)} \quad \textbf{Equation 28.}$$

The simplified energy balance for non-stratified tanks is.

$$MC_p \frac{T_{w,i+1} - T_{w,i}}{\Delta t} = m_{sup} C_p T_{sup} - m_{load} C_p T_w + m_r (h_2 - h_3) \dot{} - U_t A_t \dot{} (T_w - \dot{T}_{at}) - C_p T_w (m_{sup} - m_{load}) \quad \textbf{Equation 29.}$$

The electrical efficiency that occurs in the collector can be described as

$$\eta_{ele} = \frac{Q_e}{SA_c} \quad \textbf{Equation 30.}$$

While the thermal efficiency can be written as

$$\eta_{therm} = \frac{Q_u}{SA_c} \quad \textbf{Equation 31.}$$

Lastly, the coefficient of performance is the useful heat extracted by the collector divided by the compressor work.

$$COP = \frac{Q_u}{W_c} \quad \textbf{Equation 32.}$$

The heat pump ratio represents the amount of energy that is transferred to the water in the water tank by the heat pump to the total required to reach the water set point temperature of 50°C.

$$r_{HP} = \frac{Q_u}{Q_{Total}} \quad \textbf{Equation 33.}$$

Q_{Total} is the total heat required to raise the water temperature to 50 °C. The auxiliary heating ratio is the amount of energy required to increase the water temperature to 50 °C after the heat pump uses solar radiation to warm the water in the tank in cases of insufficient solar energy.

$$r_{AUX} = \frac{Q_{Total} - Q_u}{Q_{Total}} \quad \textbf{Equation 34.}$$

VALIDATION

The MATLAB model developed through this work were compared with the work of Ji et al.[29] The validation was completed using the same conditions, i.e. the average hourly solar and ambient temperature data for Hefei, Central China, on the day of the experiments in November. The wind speed used in our simulation for this validation was a constant average wind velocity of 3.05 m/s. However, the original study used a wind profile between 2.4 and 3.7 m/s; since this profile was not given in the paper, an average constant value was taken.

Figure 6 shows the comparison of the current study's COP with the COP from Ji et al.[29] As shown, there is excellent agreement between our results and those in this study, with a maximum deviation of 7.3% and an average root mean square error of 2.4%

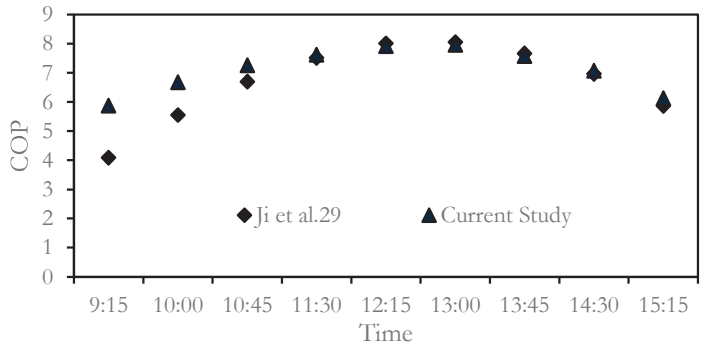

Figure 6. COP variation over time for Ji et al.[29] study and our current study

Figure 7 shows the electrical efficiency over time in comparison with Ji et al.[29] As shown, the same trend is observed with a maximum deviation of 12.0% and an average root mean square error of 5.1 %. This difference is likely due to the difference in operating conditions during experiments such as wind speed which was not presented in the study, and had been assumed constant in this model. Another possible source of deviation is the difference in the temperature coefficient of the photovoltaic cells used in the simulation. The study didn't indicate their temperature coefficient. It could also be due to startup and shutdown issues during the experiment, as the highest deviations are indicated at these times. Overall, the same trend is shown, and the average root mean square error is reasonable.

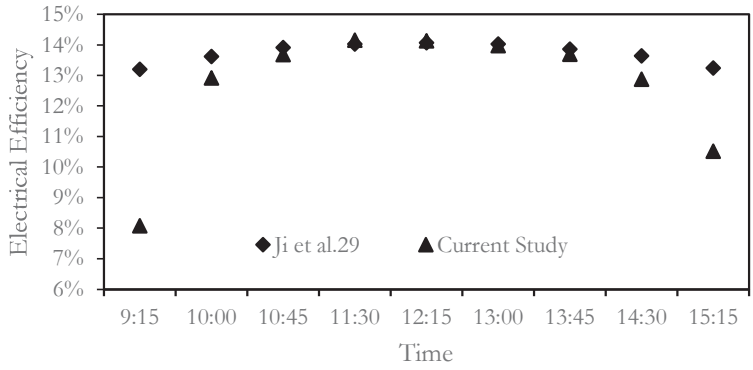

Figure 7. Electrical efficiency variation over time for Ji et al.[29] study and our current study

RESULTS & DISCUSSION

In this section, the COP, electrical efficiency, thermal efficiency, heat pump ratio and axillary heat ratio of the PVT-DXSAHP with different types of photovoltaic cells on solar collector plates are presented and discussed.

On a sunny day in winter, the COP increases as the day approaches noon, as shown in **Figure 8**. The data points show a parabolic rise in COP as it approaches noon time and then drops or rises depending on the time of the day (morning or evening). This is mainly because as time approaches noon, more solar radiation is received by the collector. This increases the amount of the collector's useful thermal energy. As the collector's useful thermal energy increases, it raises the evaporator temperature (line 4-1) in Figure 2, decreasing the amount of compressor work required to reach the condenser pressure according to **Equation (4)**. Both effects lead to an increase in the COP, as inferred by **Equation (32)**. Regarding the variation of COPs for the different solar cells, the cells which have the lowest electrical efficiency provide a larger useful heat gain of the collector than cells with higher collector efficiency, refer to **Equation (21**). The average COP on a sunny winter day for ®LG, ®Prime, ®VOLT and ®VSUN collector solar cells are, respectively, 3.91, 3.83, 3.88, and 3.92. The highest COP is provided by ®Solartech collector solar cells at 4.08.

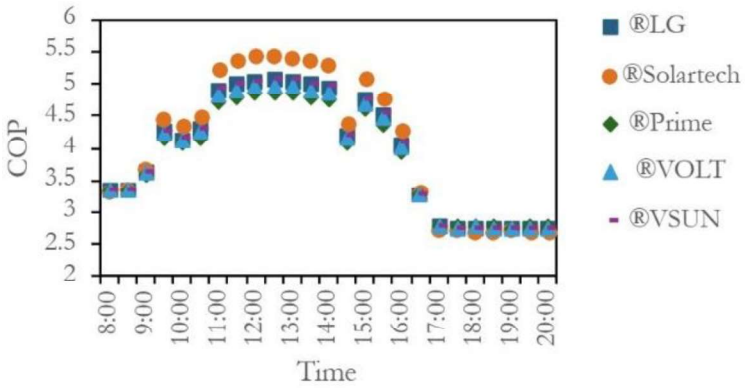

Figure 8. COP variation over time, with 5 different solar collector cells. On a sunny day in winter

The electrical efficiency of the photovoltaic cells on a sunny winter day increases parabolically as it approaches noon, as shown in **Figure 9**. Although it is a very flat parabolic maxima, each set of data points has its highest values at noon and drops during the morning and evening. This variation is because the modified solar radiation increases the amount of energy that is available for extraction by the photovoltaic cells at noon, according to **Equation (24)**. The drop in the electrical efficiency across every type of photovoltaic cell is due to the manufacturing of these cells. We can see that using ®LG, ®VOLT, ®VSUN and ®Prime gives a higher electrical efficiency because they are all mono-type solar cells, while the ®Solartech is a poly-type of solar cells. The daily average electrical efficiency on a sunny winter day for ®LG, ®Solartech, ®VOLT, and ®VSUN collector solar cells are, respectively, 12.5%, 8.3%, 13.2% and 12.2%. The highest daily electrical efficiency is provided by ®Prime collector solar cells at 14.4%.

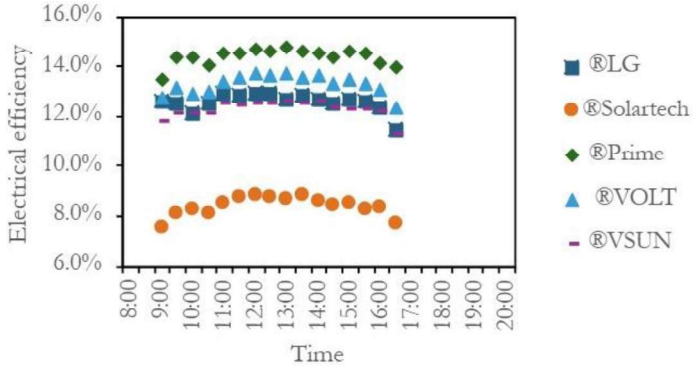

Figure 9. Variation of the electrical efficiency variation over time with 5 different solar collector cells on a sunny day in winter.

Figure 10 shows the thermal efficiency with time. As shown, during a sunny winter day, the thermal efficiency slightly decreases as it approaches noon and increases after that. As solar radiation increases as the day approaches noon, the ambient and collector temperatures increase, leading to higher heat transfer losses from the collector. This increase in photovoltaic temperature and ambient temperature raises the radiative and convective heat transfer losses, increasing the total heat loss coefficient and thereby decreasing thermal efficiency. The daily thermal efficiencies on a sunny day in winter for ®LG, ®Prime, ®VOLT, and ®VSUN collector solar cells are, respectively, 27.1%, 25.5%, 26.6 % and 27.3 %. The highest daily thermal efficiency is given by ®Solartech solar cells at 30.6%. The combined solar PVT- heat pump system differs in thermal efficiency for the different solar cells used. As the electrical efficiency of the solar cells decreases across selected solar cells, the modified useful heat gain of the collectors will increase accordingly. This increase in the modified useful heat of the collector causes an increase in thermal efficiency according to **Equation (31)**.

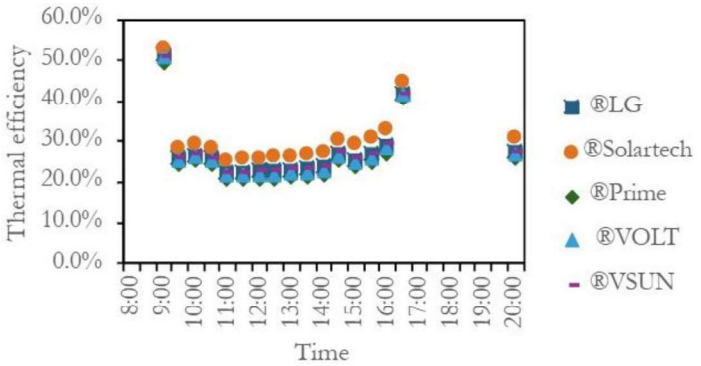

Figure 10. Variation of thermal efficiency with 5 different solar collector cells on a sunny day in winter.

Looking at a sunny day in the summer, the COP follows a decreasing trend but is larger than the COP on sunny winter days, as shown in **Figure 11**. The data sets show a decreasing trend from the start of the day to the end of the day. This is because there is sufficient heat from the outdoor air and solar radiation to heat the water to high temperatures. As the water temperature increases, the condenser temperature increases, requiring more compressor work and, thus, lower COPs. In the summer, the sun's rays are more direct during the summer in the northern hemisphere. The daily average COP on a sunny day in summer for ®LG, ®Prime, ®VOLT, and ®VSUN collector solar cells are, respectively, 7.46, 7.21, 7.33, and 7.48. The highest daily COP is provided by ®Solartech collector solar cells at 7.91. Again, the cells with the highest electrical efficiency yield the highest coefficient of performance (COP).

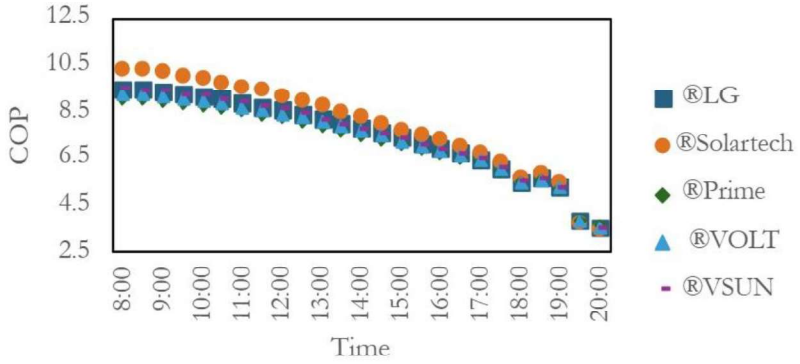

Figure 11. COP variation over time for 5 different solar collector cells on a sunny summer day.

The electrical efficiency of the solar cells in **Figure 12** follows the same trend as the solar cells in winter. However, the electrical efficiency is higher in the summer than in the winter. Comparing the meteorological data of a sunny winter and summer day in **Figure 3** and **Figure 4**, there are larger values of solar radiation on a sunny summer day compared to a sunny winter day for the 12-hour simulation. This leads to higher photovoltaic energy being collected, thus increasing the electrical efficiency according to **Equation (30)**. The other likely reason for higher efficiencies in the summer is the lower thermal losses and the more useful heat gain from the outdoor air, according to **Equation (24)**. The daily average electrical efficiencies on a sunny summer day for ®LG, ®Solartech, ®VOLT, and ®VSUN collector solar cells are, respectively, 14.9%, 11.2%, 15.7% and 14.6%. The highest daily electrical efficiency is provided by ®Prime collector solar cells at 16.5%, which has the lowest coefficient.

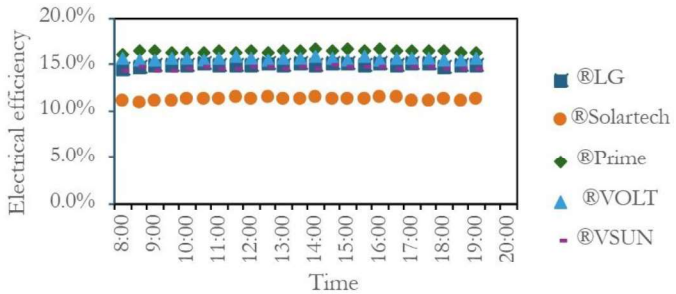

Figure 12. Electrical efficiency as a function of time for 5 different solar collector cells on a sunny day in summer.

Figure 13 shows the thermal efficiency for a sunny summer day. This trend is similar to the thermal efficiency in **Figure 9**. However, the thermal efficiency is higher in the summer than on a sunny winter day. Higher solar radiation, higher outdoor air temperatures and lower thermal losses contribute to the efficient operation of the collector. The daily thermal efficiencies on a sunny day in winter for ®LG, ®Prime, ®VOLT, and ®VSUN collector solar cells are, respectively, 50.6%, 48.1%, 49.3% and 50.9%. The highest daily thermal efficiency is provided by ®Solartech collector solar cells at 55.4%. As previously discussed, the lower the solar cell's electrical efficiency is, the larger the system's thermal efficiency will be.

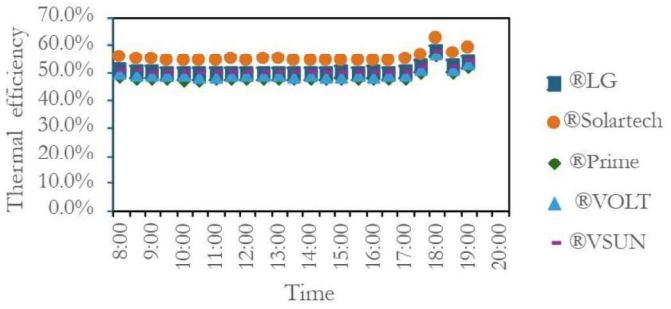

Figure 13. Thermal efficiency variation over time for 5 different solar collector cells on a sunny day in summer.

The COP on a cloudy summer day contains a scattered distribution trend which rises and falls at certain times of the day. This is shown in **Figure 14**, the data sets peak at 9:00, 11:00, 12:15 and 15:30 and drop after those times and rise again. This distribution can be explained by the fact that at some points in the day, shown in **Figure 5**, cloud cover occurs, and the solar radiation drops at those points in time, reducing the useful energy gain from the collector and thus reducing heat pump COP. The daily average COP on a cloudy day in summer for ®LG, ®Solartech, ®VOLT and ®VSUN collector solar cells are, respectively, 6.16, 6.02, 6.10, and 6.18. The highest daily COP is provided by ®Prime collector solar cells at 6.45.

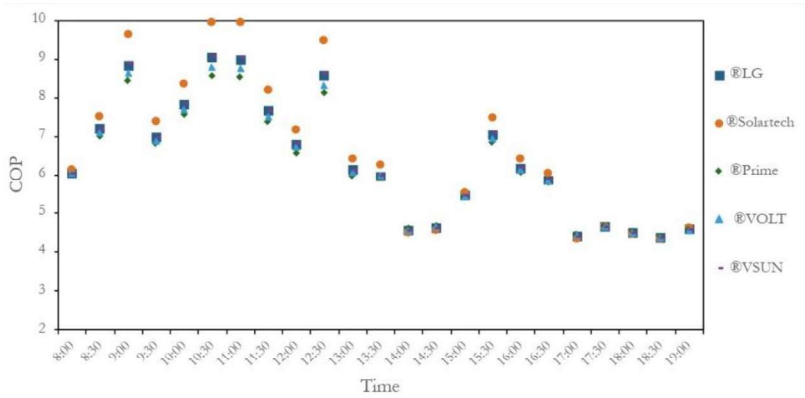

Figure 14. COP variation over time for 5 different solar collector cells on a cloudy day in summer.

The electrical efficiency of the collector on a cloudy shown in **Figure 15**, has a similar trend as that on a sunny summer. However, there are times when the electrical efficiency is zero at some points in the day due to cloud cover totally obstructing the sun above the collector, thus leading to very little or almost no solar energy reaching the photovoltaic cells. The daily average electrical efficiencies on a cloudy day in summer for ®LG, ®Solartech, ®VOLT and ®VSUN collector solar cells are 12.0, 8.7, 12.7 and 11.8 %, respectively. The highest daily electrical efficiency is provided by ®Prime collector solar cells at 13.6 %.

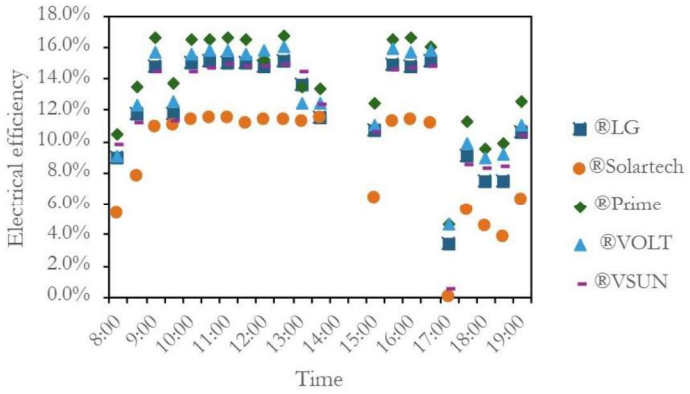

Figure 15. Electrical efficiency variation over time for 5 different solar collector cells on a cloudy day in summer.

The thermal efficiency of the collector on a cloudy day, shown in **Figure 16,** can be described as a random distribution that follows the solar radiation earlier presented. The thermal efficiency randomly fluctuates, following the trend of solar radiation. Cloud cover causes a drop in the solar energy reaching the collector. This results in a rise in thermal efficiency because as the solar radiation decreases, the thermal efficiency increases, according to **Equation (31)**. This is in part because the solar collector is able to utilize the outdoor air to provide useful heat gain even when there is no solar radiation. Their ability to absorb energy from outdoor air is one of the reasons direct-expansion solar-assisted heat pumps are advantageous compared to traditional solar collectors. Thus, every time cloud cover is present, the efficiency rises, and then when clouds do not obstruct the sun, the data will resemble thermal efficiency values close to those of a sunny summer day in **Figure 13**. The daily average thermal efficiencies on a cloudy day in summer for ®LG, ®Prime, ®VOLT, and ®VSUN collector solar cells are, respectively, 61.3, 58.3, 60.0and 61.8%. The highest daily thermal efficiency is provided by ®Solartech collector solar cells at 67.4%.

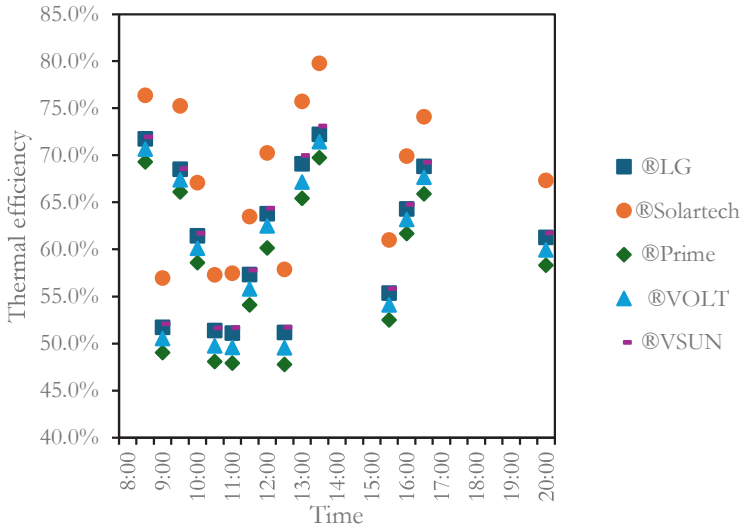

Figure 16. Thermal efficiency variation over time for 5 different solar collector cells on a cloudy summer day.

The heat pump ratio is defined as the ratio of the energy delivered by the heat pump to the total energy required to heat the water to its target temperature. As expected, this value is the lowest for sunny winter days and the highest for sunny summer days. **Table 2** shows the heat pump ratio for the considered summer and winter conditions. This is because the availability of solar radiation on sunny summer days is greater than the cloudy days and sunny winter days, as shown in **Figures 3** to **5**. The more the available solar radiation, the higher the energy supplied to the heat pump to heat the refrigerant to heat the water in the tank and the less the auxiliary heat required. Thus, a higher heat pump ratio is desired to ensure that most of the heat is supplied by the more efficient heat pump system rather than the less efficient auxiliary heating system.

The same variation is expected for the auxiliary heat ratio. It is lowest on a sunny summer day and the highest on a sunny winter day, as shown in **Table 2**. The sun's availability on sunny winter days is lower than on cloudy and sunny summer days. This leads to less solar radiation collected by the collector and used in the heat pump, requiring he compressor to work harder in order to reach the refrigerant temperature necessary to heat the water in the water tank. Therefore, a lower auxiliary heat ratio is desirable, as it indicates that less auxiliary heat is required to raise the water temperature to its desired value.

	Heat pump ratio	Auxiliary heat ratio
Cloudy Summer	38.2%	66.0%
Sunny Winter	15.6%	86.7%
Sunny Summer	49.0%	57.1%

Table 2. Heat pump ratio and Auxiliary heat ratio average across all solar collector cells on the three 12 hour simulated days for all solar cells

Looking at the difference in the performance parameters across all the photovoltaic cells. The COP of the highest to lowest system differs by about 0.7 across each of the three types of days considered. The thermal efficiency of the photovoltaic cells differs by about 6% from the highest to the lowest thermal efficiency over the three types of days considered. It is evident from the foregoing discussion that the solar cells, which give the highest COP and thermal efficiency for the heat pump across the three types of days, show noticeable differences in the performance parameters. When identifying the most effective photovoltaic cell to use in the PV-DXSAHP, over the three types of days considered in this study, the ®Prime cells are advantageous over the other PV cells for the PV-DXSAHP system owing to their higher electrical efficiency. The solar cells have a larger electrical efficiency than the rest of the solar cells and remain within a maximum of 0.7 and 6% range of COP and thermal efficiency, respectively, compared with the other solar cells.

CONCLUSION

In this study, a detailed thermodynamic model of a solar photovoltaic-thermal-direct expansion solar-assisted heat pump was developed and validated. Using the developed model, the performance of the system in cold climates was undertaken for different commercially available solar cells. The solar collector cells that provided the largest COP were the ®Solartech cells, electrical efficiency was the ®Prime cells, and thermal efficiency was the ®Solartech cells. At the end of a 12-hour simulation, the average heat pump ratio was 38.2% on a cloudy summer day, 15.6% on a sunny winter day and 49.0% on a sunny summer day. The average axillary heat ratio was 66.0% on a cloudy summer day, 86.7% on a sunny winter day and 57.1% on a sunny summer day. Overall, results show that the solar cells with the lowest electrical efficiencies gave the higher COP across all three days.

ACKNOWLEDGMENTS

I want to acknowledge the students in the Sustainable Thermal Energy Systems Research Lab at the University of Calgary, Bardia Abbasi, for his guidance and the NSERC Undergraduate Student Research Award for giving me the opportunity to undertake this work.

NOMENCLATURE

$\bar{Q}_u$	modified useful energy gain (W)
$\bar{m}_r$	mass flow rate of refrigerant (kg/s)
ρ_r	density of the refrigerant (m^3/kg)
h_1	enthalpy of refrigerant exiting the collector (kJ/kg)
h_4	enthalpy of refrigerant entering the collector (kJ/kg)
η_{vol}	volumetric efficiency of refrigerant (unitless)
P_c	pressure in the condenser of the heat pump (kPa)
P_{eva}	pressure in the evaporator of the heat pump (kPa)
n	speed of the compressor (rpm)
V_d	volumetric displacement of compressor (m^3)
$h_{r,PV-amb}$	radiative heat transfer coefficient with Photovoltaic cells and ambient air (W/m^2K)
ε_{PV}	emissivity of Photovoltaic cells (-)
σ	Stephan-Boltzmann constant (W/m^2K^4)
T_{PV}	photovoltaic cell temperature (K)
T_{amb}	ambient air temperature (K)
$h_{c,PV-amb}$	convective heat transfer coefficient with Photovoltaic cells and ambient air (W/m^2K)
u_{amb}	wind speed of ambient air (m/s)
R_{r-c}	heat resistance from ambient across ambient air to Photovoltaic cells (m^2K/W)
R_{PV}	heat resistance across Photovoltaic cells (m^2K/W)
δ_{PV}	photovoltaic cell thickness (m)

k_{PV}	thermal conductivity of photovoltaic cell (W/mK)
U_{Bottom}	back loss coefficient (W/m²K)
k_b	thermal conductivity of back insulation (W/mK)
δ_b	thickness of back insulation (m)
U_L	total heat loss coefficient (W/m²K)
η_c	collector efficiency (%)
η_r	collector reference efficiency (%)
β_r	photovoltaic temperature coefficient (1/K)
T_r	reference temperature of the photovoltaic cell (K)
η_{amb}	collector efficiency at ambient temperature (K)
$\bar{U}_L$	modified total heat loss coefficient (W/m²K)
S	solar radiation (W/m²)
α	absorptivity of photovoltaic (-)
$\bar{S}$	modified solar radiation (W/m²)
h_{fi}	coefficient of heat transfer of two-phase refrigerant (W/m²K)
k_l	thermal conductivity of refrigerant (W/mK)
D_i	Internal diameter of the absorber tube (m)
Re	Reynolds number (-)
J	design constant (-)
L	length of the absorber tube across collector (m)
Δx	quality difference inlet and outlet of collector (-)
h_{fg}	latent heat of refrigerant (W/m²K)
F'	collector efficiency factor (-)
W	distance between each row of absorber tube in the collector (m)
F	fin efficiency parameter (-)
C_b	conduction bound of absorber tube to absorber plate (W/mK)
D	outer diameter of the absorber tube (m)
h_{fi}	heat transfer coefficient between the fluid and the tube walls (W/m²K)
m	boundary condition constant (-)
k_p	thermal conductivity of the absorber plate (W/mK)
δ_P	thickness of the absorber plate (m)
A_c	area of the collector (m²)
T_p	temperature of the absorber plate (K)
T_e	evaporating temperature (K)
W_c	compressor work (W)
h_2	enthalpy of refrigerant exiting the compressor (kJ/kg)

h_1	enthalpy of refrigerant entering the compressor (kJ/kg
η_{is}	isentropic efficiency of the compressor (%)
Q_c	useful energy transferred from the condenser to the water tank via heat exchanger (W)
$\dot{m}_w$	mass flow rate of water into the tank (kg/s)
C_p	heat capacity of water (kJ/K)
T_{wo}	temperature of outlet water of heat exchanger (K)
T_w	water tank temperature (K)
U_c	heat loss coefficient at the condenser (W/m²K)
A_C	area of the condenser (m²)
ΔT_{lm}	log-mean temperature difference (K)
T_2	temperature exiting the compressor (K)
T_c	condenser temperature (K)
M	water mass in the tank (kg)
$T_{w,i+1}$	load water temperature next time step (K)
$T_{w,i}$	load water temperature current time step (K)
Δt	timestep (s)
$\dot{m}_{\text{sup}}$	mass flow of water load supplied to the water tank (kg/s)
T_{sup}	supplied water temperature (K)
$\dot{m}_{load}$	mass flow of water load exiting the water tank (kg/s)
U_t	heat loss coefficient of water tank (W/m²K)
A_t	area of the water tank (m²)
T_{at}	air temperature surrounding the water tank (K)

REFERENCES

1. Natural Resources Canada, 2019 Survey of Household Energy Use (SHEU-2019) Data Tables, *https://oee.nrcan.gc.ca/corporate/statistics/neud/dpa/showTable.cfm?type=SH&sector=aaa&juris=ca&year=2019&rn=63&page=1* (accessed August 2024)
2. Natural Resources Canada, Residential Sector - GHG Emissions, *https://oee.nrcan.gc.ca/corporate/statistics/neud/dpa/showTable.cfm?type=AN&sector=aaa&juris=00&year=2021&rn=2&page=0* (accessed August 2024)
3. Elgamal N, Sambi J, Patel D, Marasinghe C, Pulikkottil E, Virtusio K, Mwesigye A, Li S. Design. (2022) Construction, and Thermodynamic Analysis of a Direct-Expansion Solar Assisted Heat Pump for Cold Climates, *Energy. American Society of Mechanical Engineers 6*, 1-10. *https://doi.org/10.1115/IMECE2022-95940*
4. Abbasi B, Li S, Mwesigye A. (2024) Experimental investigation of the thermal performance of a prototype direct-expansion solar-assisted heat pump system in a cold climate, *Conference on Energy Sustainability, ASME 18th proceeding, https://doi.org/10.1115/ES2024-126975*
5. Sun X, Wu J, Dai Y, Wang R. (2014) Experimental study on roll-bond collector/evaporator with optimized-channel used in direct-expansion solar assisted heat pump water heating system, *Applied Thermal Engineering 66*, 571-579. *https://doi.org/10.1016/j.applthermaleng.2014.02.060*

6. Huang BJ, Lee JP, Chyng JP. (2005) Heat-pipe enhanced solar-assisted heat pump water heater, *Solar Energy 78,* 375-381. *https://doi.org/10.1016/j.solener.2004.08.009*

7. Chow TT, He W, Ji J. (2007) An experimental study of façade-integrated photovoltaic/water-heating system, *Applied Thermal Engineering 27*, 37-45. *https://doi.org/10.1016/j.applthermaleng.2006.05.015*

8. Nagano K, Mochida T, Shimakura K, Murashita K, Takeda S. (2003) Development of thermal-photovoltaic hybrid exterior wallboards incorporating PV cells in and their winter performances, *Solar Energy Materials and Solar Cells 77,* 265-282. *https://doi.org/10.1016/S0927-0248(02)00348-3*

9. Kostić LjT, Pavlović TM, Pavlović ZT. (2010) Optimal design of orientation of PV/T collector with reflectors, *Applied Energy 87*, 3023-3029. *https://doi.org/10.1016/j.apenergy.2010.02.015*

10. Kalogirou SA, Tripanagnostopoulos Y. (2006) Hybrid PV/T solar systems for domestic hot water and electricity production, *Energy Conversion and Management 47*, 3368-3382. *https://doi.org/10.1016/j.enconman.2006.01.012*

11. Kazem HA, Al-Waeli AHA, Chaichan MT, Al-Waeli KH, Al-Aasam AB, Sopian K. (2020) Evaluation and comparison of different flow configurations PVT systems in Oman: A numerical and experimental investigation, *Solar Energy 208,* 58-88. *https://doi.org/10.1016/j.solener.2020.07.078*

12. Poredoš P, Tomc U, Petelin N, Vidrih B, Flisar U, Kitanovski A. (2020) Numerical and experimental investigation of the energy and exergy performance of solar thermal, photovoltaic and photovoltaic-thermal modules based on roll-bond heat exchangers, *Energy Conversion and Management 210,* Article 112674. *https://doi.org/10.1016/j.enconman.2020.112674*

13. Huang BJ, Chyng JP. (1999) Integral-type solar-assisted heat pump water heater, *Renewable Energy 16*, 731-734. *https://doi.org/10.1016/S0960-1481(98)00264-X*

14. Ammar AA, Sopian K, Alghoul MA, Elhub B, Elbreki AM. (2019) Performance study on photovoltaic/thermal solar-assisted heat pump system, *Journal of Thermal Analysis and Calorimetry 136*, 79-87. *https://doi.org/10.1007/s10973-018-7741-6*

15. Ji J, He H, Chow T, Pei G, He W, Liu K. (2009) Distributed dynamic modeling and experimental study of PV evaporator in a PV/T solar-assisted heat pump, *International Journal of Heat and Mass Transfer 52*, 1365-1373. *https://doi.org/10.1016/j.ijheatmasstransfer.2008.08.017*

16. Vaishak S, Bhale P V. (2021) Performance analysis of a heat pump-based photovoltaic/thermal (PV/T) system, *Clean Technologies and Environmental Policy* 23, 1121-1133. *https://doi.org/10.1007/s10098-020-01839-6*

17. James A, Srinivas M, Mohanraj M, Raj AK, Jayaraj S. (2021) Experimental studies on photovoltaic-thermal heat pump water heaters using variable frequency drive compressors, *Sustainable Energy Technologies and Assessments 45*, Article 101152. *https://doi.org/10.1016/j.seta.2021.101152*

18. LG, LG NeON®H*, https://cdn.shopify.com/s/files/1/0497/4749/3026/files/LG_NeON_H_*. (accessed August 2024)

19. SOLARTECH® POWER, INC. M-series 5W PV Module SPM005P-R, *https://www.solartechpower.com/images/Mseries/SPM005P-R.pdf.* (accessed August 2024)

20. SunPower, SunPower® Flexible Solar Panels | SPR-E-Flex-110, *https://sunpower.global/int/sites/default/files/2019-10/sp_E_Flex_110W_UK.pdf.* (accessed August 2024)

21. Volts Energies, Technical Data sheet V200M-48V-G1, *https://solarelios.com/wp-content/uploads/2024/01/Technical_Data_sheet_V200M-48V-G1-_Volts-Energies.pdf.* (accessed August 2024)

22. VSUN, VSUN480N-120BMH-DG-BW*, https://cdn.enfsolar.com/z/pp/u3f3b7jkz/20211029100136044.pdf?_gl=1*1b38px4*_gcl_au*MjEwODA1NzUwOC4xNzQxMjIzODU3*.* (accessed August 2024)

23. Abbasi B. (2023) Thermodynamic Investigation of Solar-Assisted Heat Pumps for Water Heating Applications in Cold Climatic Conditions*, https://doi.org/10.11575/PRISM/42588*

24. Florschuetz LW. (1976) Extension of the Hottel-Whillier model to the analysis of combined photovoltaic/thermal flat plate collectors, *Solar Energy 22*, 361-366. *https://doi.org/10.1016/0038-092X(79)90190-7*

25. Brunin O, Feidt M, Hivet B. (1997) Comparison of the working domains of some compression heat pumps and a compression-absorption heat pump, *International Journal of Refrigeration 20*, 308-318. *https://doi.org/10.1016/S0140-7007(97)00025-X*

26. Duffie, A.J., and Beckman, A.W. (2013) Flat-Plate Collectors, in *Solar Engineering of Thermal Processes* 4th ed., 236 – 321, John Wiley & Sons.

27. Soteris, AK. (2009) Photovoltaic Systems, in *Solar energy engineering: Processes and Systems* 1st ed., 504, Elsevier/Academic Press

28. Turaga M, Guy RW. (1985) Refrigerant side heat transfer and pressure drop estimates for direct expansion coils. A review of works in North American use, *International Journal of Refrigeration 8*, 134-142. https://doi.org/10.1016/0140-7007(85)90152-5

29. Ji J, Liu K, Chow T tai, Pei G, He W, He H. (2008) Performance analysis of a photovoltaic heat pump, *Applied Energy 85*, 680-693. *https://doi:10.1016/j.apenergy.2008.01.003*

ABOUT STUDENT AUTHOR

Adam Anastas is a mechanical engineering student graduating in June of 2025.

PRESS SUMMARY

This study investigates the performance of a heat pump driven by solar radiation using various types of photovoltaic cells on the evaporator of the heat pump. A mathematical model was developed to understand how well the heat pump increases the temperature of water used in residential homes in cold climates.